Biophysical Chemistry 135 (2008) 19–24

Contents lists available at ScienceDirect

Biophysical Chemistry

journal homepage: http://www.elsevier.com/locate/biophyschem

Study on the mechanism of the BtuF periplasmic-binding protein for vitamin B_{12}

Ming Liu [a], TingGuang Sun [a], JianPing Hu [a,b], WeiZu Chen [a], CunXin Wang [a,*]

[a] College of Life Sciences and Bioengineering, Beijing University of Technology, Beijing 100022, China
[b] Department of Chemistry and Life Science, Leshan Normal University, Leshan 614004, China

ARTICLE INFO

Article history:
Received 13 November 2007
Received in revised form 27 February 2008
Accepted 28 February 2008
Available online 6 March 2008

Keywords:
Molecular dynamics simulation
Steered molecular dynamics
Potential of mean force
Principal component analysis
BtuF

ABSTRACT

BtuF is the periplasmic binding protein (PBP) that binds vitamin B_{12} and delivers it to the periplasmic surface of the ABC transporter BtuCD. PBPs generally exhibit considerable conformational changes during ligand binding process, however, BtuF belongs to a subclass of PBPs that, doesn't show such behavior on the basis of the crystal structures. Employing steered molecular dynamics on the B_{12}-bound BtuF, we investigated the energetics and mechanism of BtuF. A potential of mean force along the postulated vitamin B_{12} unbinding pathway was constructed through Jarzynski's equality. The large free energy differences of the postulated B_{12} unbinding process suggests the B_{12}-bound structure is in a stable closed state and some conformation changes may be necessary to the B_{12} unbinding. From the result of the principal component analysis, we found the BtuF-B_{12} complex shows clear opening-closing and twisting motion tendencies which may facilitate the unbinding of B_{12} from the binding pocket. The intrinsic flexibility of BtuF was also explored, and it's suggested the Trp44-Gln45 pair, which is situated at the mouth of the B_{12} binding pocket, may act as a gate in the B_{12} binding and unbinding process.

1. Introduction

Located between the inner and outer membrane of Gram-negative bacteria, periplasmic binding proteins (PBPs) mediate solute transport or initiate chemotaxis by activating flagellar motion [1–3]. With only one membrane, Gram-positive bacteria employ a similar but membrane-anchored version of PBPs [4,5]. PBPs bind many kinds of substrates ranging from sugars, amino acids, and peptides to a variety of ion compounds and vitamins [6]. Accordingly, the PBP family consists of many proteins with rather diverse sequences. Despite obvious diversity in their primary structure, all PBPs share a similar tertiary structure: two globular domains connected by a variably linker. On the basis of the similarities in primary structure [2,7] or by the topology of their globular domains [8–10], PBPs can be divided into three classes which are characterized by the number of the linker connecting the two lobes. Three groups have been identified so far, and group I, II, III have three, two, and one interconnection domains, respectively [3,11].

BtuF is the periplasmic binding protein in the vitamin B_{12} uptake system in *E.* coli, which to date is the only import system with crystal structures of all its key components available [12,13]. The whole uptake system is composed of BtuB [14], BtuF [11,15] and BtuCD [16]. BtuCD is the inner membrane transporter mediating B_{12} uptake, which falls into the ATP-binding cassette (ABC) transporter family [16]. The ABCs are involved in diverse processes such as nutrient uptake, protein secretion, drug and antibiotic resistance, antigen presentation, etc. [17–20]. On the basis of biochemical data and the structures of full ABC transporters determined in recent years, a possible docking model of BtuCDF has been suggested by Borths and co-workers, revealing that two negatively charged "knobs" near the apex of each BtuF lobes and two positively charged "pockets" on the periplasmic surface of BtuC may form interprotein salt bridges (Fig. 1) that are critical for proper interaction between BtuF and BtuC [11]. Inspiringly, this docking model has been proved recently, and the crystal structure of the BtuCDF complex in the post-translocation state has been reported [21].

Characterized by its single linker (Fig. 1), BtuF undoubtedly falls into the third group, and only tiny differences are observed between the B_{12}-bound and -free crystal structures [11,15]. Suggested by crystal structures, the two lobes of PBPs belonging to group I and II will twist and get close during the substrate binding process, and eventually enclose the ligand, resembling a Venus flytrap [1]. Without large conformational differences observed in crystal structures, the PBPs of group III, however, seem to employ a different working mechanism [22]. Nevertheless, a different voice emerges from a recent work [13], which suggested the conformational changes of BtuF may be larger than previously assumed, and the B_{12}-bound structure is in the closed state. According to Kandt's results [13], the mechanism of BtuF capturing B_{12} is associated with the model raised by Byung-Ha Oh and coworkers [23]. Despite these advances, both of the functional details of BtuF and the mechanism of B_{12} translocation process remain elusive.

Against these backgrounds, we want to explore the working mechanism of BtuF further. We applied SMD simulation on the BtuF-B_{12} complex to explore the energetics of the B_{12} unbinding process. A PMF along a postulated pathway was successfully constructed employing Jarzynski's equality [24]. Furthermore, a principal component

* Corresponding author. Tel.: +86 10 67392724; fax: +86 10 67392837.
E-mail address: cxwang@bjut.edu.cn (C. Wang).

0301-4622/$ – see front matter © 2008 Elsevier B.V. All rights reserved.
doi:10.1016/j.bpc.2008.02.017

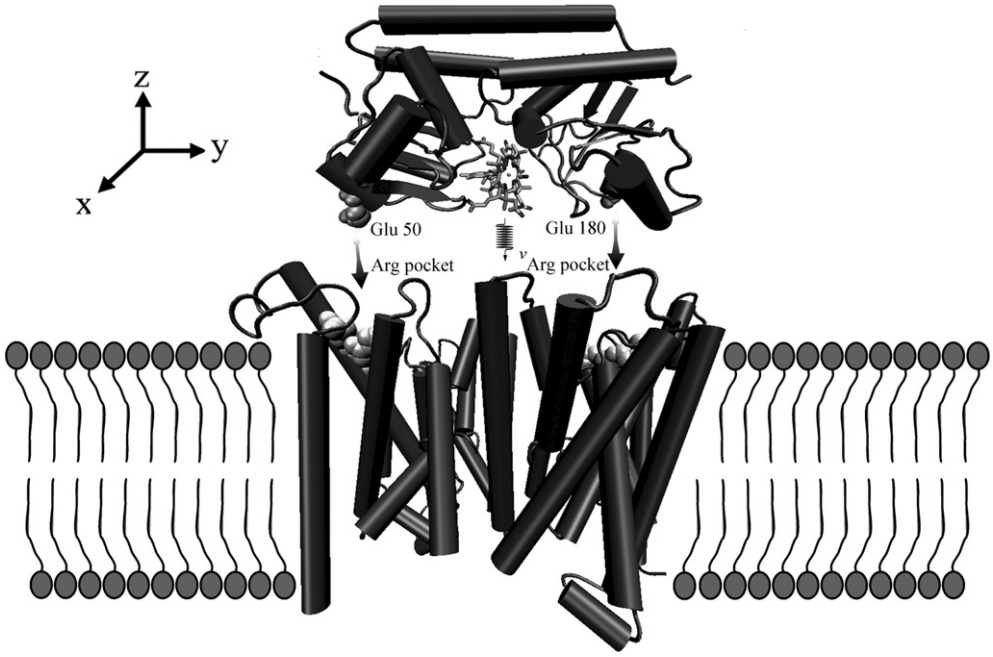

Fig. 1. The schematic of the docking model of the BtuF and BtuC. BtuF is shown by the cartoon representation in the upper part of the figure and the two negatively charged knobs, i.e. the Glu 50 at one lobe and the Glu 180 in the other, are shown by the VDW representation. BtuC is beneath the BtuF with the cartoon representation too, and the two positively charged Arg-pockets are represented by the VDW mode. The spring under the B_{12} illustrates the pulling direction in the SMD simulations is along the minus *z*-axis, which is parallel with the real B_{12} translocation pathway constituted by BtuC.

analysis (PCA) was employed to analyze the motion modes of the B_{12}-bound BtuF and the intrinsic flexibility of the BtuF was investigated too.

2. Materials and methods

2.1. Modeling

A vitamin B_{12} topology was developed for the CHARMM force field [25] using the AMBER cyanocobalamin parameters as a template [26]. The charges, inner molecular coordinates, and all force constants were obtained from the template. Altogether, five MD simulations were performed on the vitamin B_{12} alone to test the performance of the new topology. The average structure of the five test simulations is superimposed on the B_{12} crystal structure (Fig. 2) obtained from the BtuF-B_{12} complex (PDB entry: 1N4A [15]), and the average root mean square deviation (RMSD) relative to the crystal structure is 0.95 Å. The relatively small differences between the two structures reflect our topology yields a stable description for B_{12}.

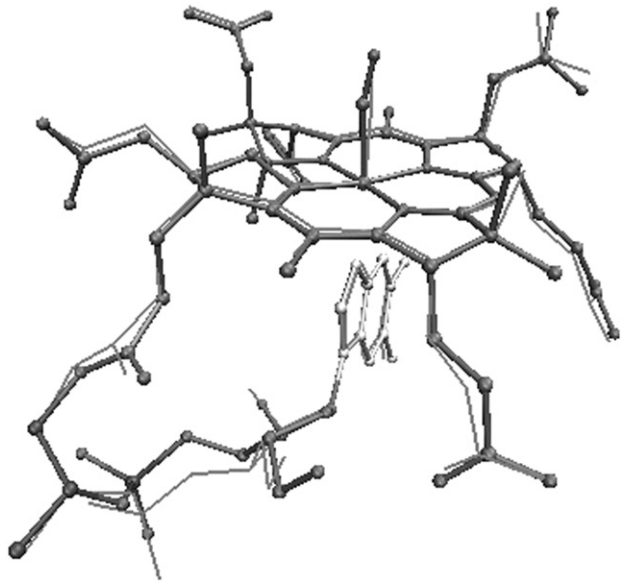

Fig. 2. Superposition of the average B12 MD structure with the crystal structure. The superimposed average structure is represented by line and the B_{12} X-ray structure is shown in the ball-and-stick representation.

In the BtuF-B_{12} MD simulation, the complex was solvated in a water box using the VMD [27] plug-in: *Solvate 1.2*, and then the system was ionized employing another plug-in *Autoionize* and the entire system holds neutral. All simulations were carried out using NAMD 2.6 [28] employing the CHARMM 27 force field [29]. All bond lengths were constrained, and the system was equilibrated for 2 ns at constant temperature (310 K) and pressure (1 atm) through Langevin piston method [30]. The C_α RMSD of the equilibrated BtuF-B_{12} complex is 0.17 nm relative to the crystal structure. After reaching equilibration, the MD simulation was continued for another 10 ns for the following analysis.

2.2. Steered molecular dynamics simulations

After manually docking BtuF onto the periplasmic surface of BtuC on the basis of the likely docking mode, the vitamin B_{12} is positioned over the entrance to the translocation pathway [11]. Therefore, the direction that is parallel to the B_{12} conduction channel constituted by BtuC was regarded as the pulling direction to model the B_{12} unbinding pathway. Without loss of generality, the B_{12} was pulled along the minus *z*-axis (Fig. 1).

In the constant velocity Steered Molecular Dynamics (*cv*-SMD) simulations,[1] a virtual spring was attached to the B_{12} center of mass (COM) and was pulled along the minus *z*-axis with the constant

[1] In constant velocity SMD simulation, the atom or the centroid of a collective atoms being pulled is called the SMD atom. At the beginning of *cv*-SMD simulation, a virtual spring with given force constant is attached to the SMD atom and a dummy atom is attached to the other side of the spring. We call the system without the virtual spring and dummy atom the former system, and the former system plus the virtual spring and dummy atom the SMD system. The dummy atom is pulled in a given velocity, and the motion of the SMD atom obviously submits to the second law of Newton and the law of Hooke.

velocity of 5×10^{-4} nm/ps. The force constant of the virtual spring is 3500 pN/nm, which is determined by trial and error according to the standard suggested by Park and colleagues [31]. The *cv*-SMD simulations were repeated four times with the same initial conditions for the potential of mean force (PMF) calculation employing Jarzynski's equality [24]. In every *cv*-SMD simulation, C_α atoms in the interconnection domain of BtuF were constrained (k=5000 pN/nm) to prevent unexpected deformations. The B_{12} molecule was slowly pulled out of the binding site along the minus z-axis for d=1.8 nm (displacement), therefore the simulation time of every *cv*-SMD simulation is d/v=3.6 ns.

Since the classical methods of free energy calculation can not be applied in nonequilibrium process, to get over this problem technically, Jarzynski's equality [24] was employed for the free energy calculation in SMD simulations. According to Jarzynski's equality [24], the external work done on a system can be associated with the free energy change of the system:

$$e^{-\beta\Delta F} = \langle e^{-\beta W} \rangle \tag{1}$$

where the average <·> is taken over the ensemble of trajectories; ΔF represents the free energy change, and W is the external work done on the system. Though the equality above is feasible theoretically, direct application of Eq. (1) is costly because the exponential average equality itself is dominated by small work values that are insufficiently sampled [32]. For practical use, the second order cumulant expansion [31] was applied for it needed only a few of trajectories:

$$\Psi_M = \frac{1}{M}\sum_{i=1}^{M} W_i - \frac{\beta}{2}\frac{M}{M-1}\left[\frac{1}{M}\sum_{i=1}^{M} W_i^2 - \left(\frac{1}{M}\sum_{i=1}^{M} W_i\right)^2\right] \tag{2}$$

where Ψ_M, M, β represents the free energy difference, the number of trajectories and $1/k_BT$, respectively, and W_i is the external work done on the former system in the ith SMD simulation. For *cv*-SMD simulations, the work done on the SMD system can be represented as:

$$W_{0\to t} = -kv\int_0^t dt' \left[\xi(r_{t'}) - \lambda_0 - vt'\right] \tag{3}$$

where ξ is the SMD atom position on a certain pathway at time $t' \in [0, t]$.

2.3. Principal component analysis

Principal component analysis (PCA) enables isolation of the essential subspace from the local fluctuations via calculation of a set of eigenvectors which describe correlated motions of atoms within the MD simulation [33]. To find out the dominant motion over a MD simulation, one can filter out all other motions by projecting the whole MD trajectory along the direction described by a selected eigenvector, and the projections of a trajectory on the eigenvectors of its covariance matrix are called principal components (pc's). It is helpful to calculate the two extreme projections on the time-averaged structure from the simulation and performing an interpolation between these extremes. In this work, the PCA is performed with Gromacs 3.3[34], and the trajectory is from the previous MD simulation on BtuF-B_{12} complex.

3. Results and discussion

3.1. The rationality of the PMF construction

As is shown by Eq. (3), one has to exclude of the elastic potential for the application of Jarzynski's equality [24], otherwise the PMF will be somewhat distorted. Instead of calculating the elastic potential, one can omit the elastic potential as long as it's small. It is not impossible to calculate the elastic potential, but a much easier way is to use a hard spring [31]. Thereby, the first thing needs to be checked is whether the elastic potential can be omitted. Due to the application of the constant velocity scheme, one can expect that the plot of the displacement of SMD atom, i.e. the COM of B_{12}, along the minus z-axis vs. simulation time should be linear and closely follows that of the displacement of the constraint position [31]. In Fig. 3A, noticing all four profiles are very close to the line representing the displacement of the constraint position, therefore the hard spring condition holds. Again, by inspecting all four simulations, it's found that the magnitude of the elastic potential is less than 15 kJ mol^{-1}, which is small compared with the magnitude of PMF. Further, the fluctuation of external work was calculated, which is often used as a measure of the applicability of Jarzynski's equality [31]. Basically, only when the fluctuation of work is comparable to the temperature, Jarzynski's equality [24] is considered practically applicable [35–37]. Here we report the standard deviation (SD) of the external work for the unbinding process of B_{12} is ca. 11.7 kJ mol^{-1}, i.e. 4.5 k_BT, which is reasonable for PMF calculation employing Jarzynski's equality [31].

3.2. Energetics of the B_{12} Unbinding

Two profiles are involved in Fig. 3B. One is the average external work with the corresponding SD as a function of the displacement of the SMD atom relative to the initial position, the other is the PMF. Fig. 3B can be roughly divided into two parts according to the SMD simulation process lies behind. In Part I (0–0.9 nm), both of the two profiles are monotone increasing, which is corresponding to the pulling process within the B_{12} binding pocket. As to the Part II (0.9–0.18 nm) representing the pulling process in water, the two profiles seem to be about to reach a plateau.

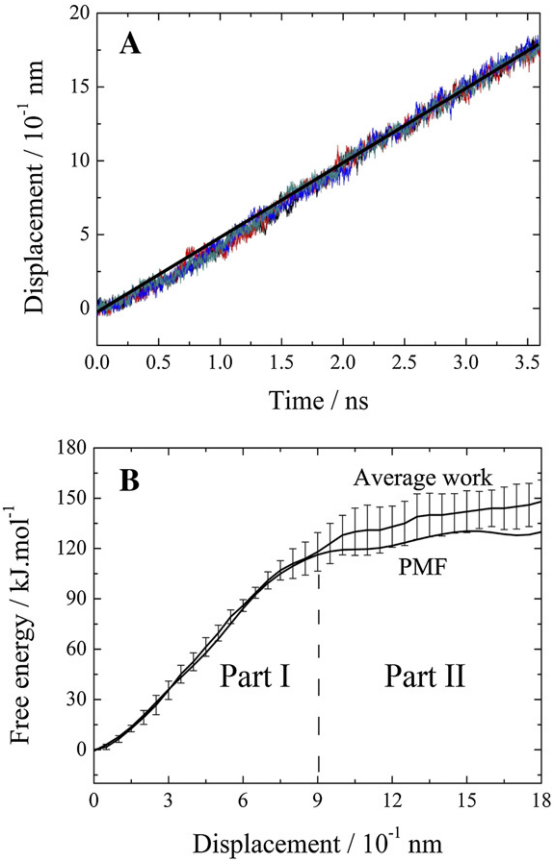

Fig. 3. PMF construction from the SMD simulations. (A) The trajectory of B_{12} COM displacement along minus z direction. Different colors represent data from different *cv*-SMD simulations (B) The PMF (lower) along the $-z$ direction and the average work profile (upper) with error bars. The bars represent the standard deviation of the external works. (For interpretation of the references to colour in this figure legend, the reader is referred to the web version of this article.)

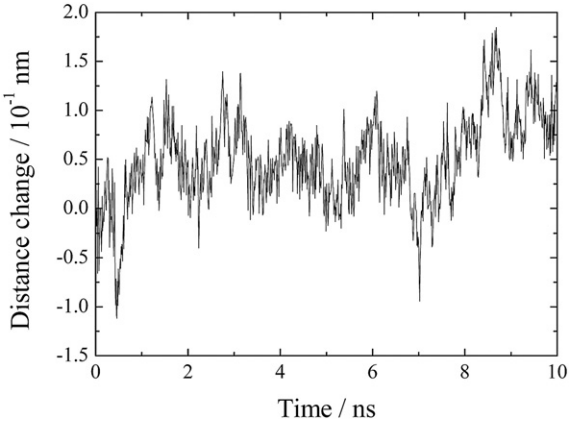

Fig. 4. The distance change between the two characteristic residues (Glu 50 and Glu 180) as a function of the simulation time. The largest fluctuation of the distance change is less than 0.2 nm over the entire simulation, suggesting the BtuF–B_{12} complex is stable.

The two profiles are hard to be distinguished in the Part I, but are distinct in the Part II. This is owing to the larger fluctuation of the external work in Part II. According to the Jarzynski's equality, the larger the external work fluctuation, the lower the corresponding PMF as long as the hard spring condition holds [31,32]. It is the relative large external work fluctuation in Part II that results in the fall of PMF. The factor causing the large fluctuation of external work in Part II is quite simple. Apparently, the motion of B_{12} in the XY plane (remembering the B_{12} was pulled along the minus *z*-axis) is constrained in a very limited range by the residues along the unbinding pathway, hence the fluctuation of the external work is very small (Fig. 3B, Part I); whereas, B_{12} is free of these constraints when is pulled in water thus results in the relatively large fluctuation of the external work in Part II. Visualizing the four SMD simulations, it is found the four trajectories of the motion of B12 are nearly coincident within the binding pocket, but are very different from each other in water (data not shown).

To some extent, PMF can reveal further structural and functional information [38]. In Part I, no local minimum is found in the PMF profile, which suggests that no favorable interactions facilitating the unbinding of B_{12} exist along the binding pocket. Considering the major function of PBPs is capturing ligand, this result is reasonable, or else the ligands will be likely to escape from the "cage" before the PBPs docking onto their cognate transporter. Although some tiny fluctuations are found in the PMF profile of the Part II, they are irrelevant to the interaction between BtuF and B_{12}.

According to the calculation on the ensemble of the external works through Jarzynski's equality [24], the free energy difference for the B_{12} unbinding is ca. 113 kJ mol^{-1}, and the free energy change over the entire pulling process is ca. 117 kJ mol^{-1}. The free energy difference between the state of the B_{12}-bound and the B_{12}-pulled-out is much larger than the previously reported BtuF-b12 binding free energy, which is around 30 kJ mol^{-1} [12]. This is not surprising since the free energy difference between the state of the B_{12}-bound and the B_{12}-pulled-out is not simply equal to the binding free energy. Basically, the free energy difference in this work represents how hard the B_{12} is released by BtuF under the current condition. Obviously, this large free energy difference suggests nearly in no case can B_{12} be released by BtuF under the current circumstance. According to results given by Kandt and colleagues, the B_{12}-bound structure is in a "closed" state [13], and the large free energy difference given by our work is just supportive to their points.

A natural guess is that the BtuF may undergo a series of conformation changes to facilitate the release of B_{12}. Based on the recently published crystal structure of BtuCDF complex, relatively large conformational changes have been observed both in the BtuF and the BtuCD [39]. Nevertheless, the crystal structure of the BtuCDF complex is in the post-translocation state, therefore, one cannot figure out whether the large conformation changes are possible in the first stage of B_{12} translocation, i.e. the B_{12} unbinding process. Further, one must notice that the BtuF-B_{12} complex is quite stable as was revealed not only by the long time multi-copy MD simulations done by Kandt and colleagues [13], but also by the PMF profile given by this work. Combined these backgrounds, it is speculated that large conformation changes of BtuF may not happen before the release of B_{12} because of the strong affinity between BtuF and B_{12}, whereas, small and stepwise conformation changes may take place after BtuF docking onto the periplasmic surface of BtuC to facilitate the release of B_{12}.

3.3. The motion modes of BtuF

Suggested by Kandt's multi-copy simulations, the conformation of the B_{12}-free BtuF fluctuates between the open and the closed state, and the BtuF-B_{12} complex stays at the closed state [13]. Though the force fields being used are different, it's still observed the similar phenomenon in our simulation. As is shown in Fig. 4, no clear opening–closing motion is observed over the 10 ns BtuF-B_{12} complex MD simulation. Though a large fluctuation occurs in the end of the simulation, the conformation of the complex is still tight and the orientation of B_{12} is identical with that in the crystal structure. Superimposing the backbone of BtuF at that frame (corresponding to the largest distance change) onto the crystal structure, the RMSD is merely 0.17 nm.

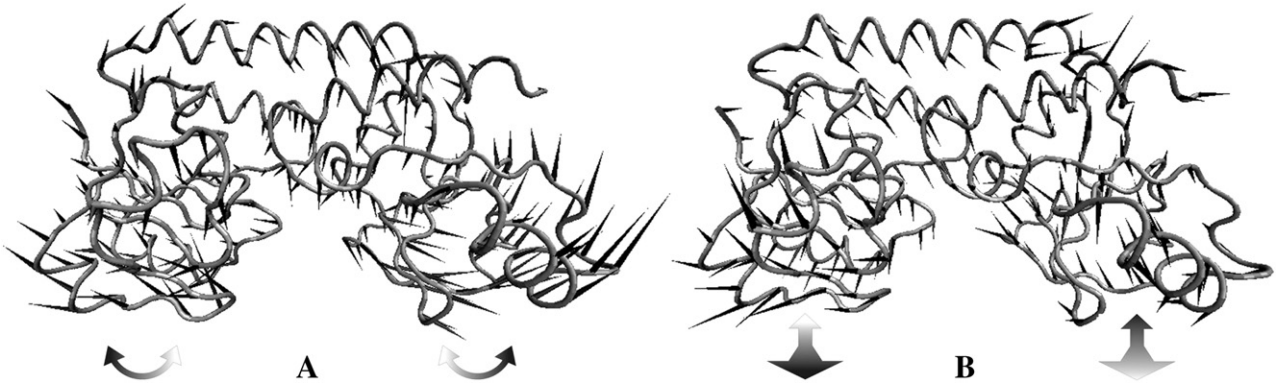

Fig. 5. Principal component analysis of the BtuF–B_{12} complex simulation. (A). Porcupine plot of the first pc (projection along the first eigenvector). (B). Porcupine plot of the second pc (projection along the second eigenvector). B_{12} is excluded from the plots for simplicity. The length of the cone in each C_α represents the magnitude of movement and the direction is from one extreme to the other.

From the results of PCA based on a series MD simulation, we learned that the B_{12}-free BtuF not only shows opening-closing motion but also the twisting motion [40]. This result is in line with those of the normal mode analysis (NMA) revealed in Kandt's work [13]. Combined with the two major observations, it is suggested that the conformation of the B_{12}-free BtuF may fluctuate between the open and the closed states and twist about the linker in the mean time. Following the similar protocol, we explored the motion modes of the BtuF-B_{12} complex in virtue of the power of PCA. The first two motion modes of the B_{12}-bound BtuF are shown in Fig. 5A and B, respectively. It's obvious that the complex still shows the opening-closing and twisting motions like the B_{12}-free BtuF. Additionally, the opening-closing motion is more prominent than the twisting motion as is suggested by the corresponding eigenvalues. Though these motions are hard to distinguish within the MD accessible time scale, the results of the PCA suggest that BtuF is more flexible than previously assumed.

3.4. The intrinsic flexibility of BtuF

After discussing the motion modes, we want to explore the flexibility of the BtuF-B_{12} complex in order to figure our which part of it contributes most to the conformation changes. Intuitively, one may expect that the largest deviation should occur nearby the two free terminals of BtuF since the BtuF-B_{12} complex is rather stable. After checking the RMSF (Fig. 6) carefully, however, it is found the most flexible regions are located at the loops which are around the mouth of the B_{12} binding site and the most rigid region was the interconnection domain (residue ID: 106–126), which roughly coincided with the experimental result [15]. Again, as a reflection of the symmetry of the structure of BtuF, the RMSF is somewhat symmetric with respect to the interconnection domain.

From Fig. 6, six large fluctuations are found: Gln45 in one lobe, and Asp 169, Arg171, Val172, Pro173 and Gly207 in the other. For the first five residues, it is of interest that all of them are located at the loops that interact with the periplasmic loops of BtuC (data not shown). Taking this fact into consideration, it's not difficult to understand the reason lies behind the exceptional flexibility of these residues. As to the Gly207, which locates far away from the B_{12} binding site, however, further works need to be done to figure out why it is abnormally flexible.

As is illustrated by Fig. 6, the most flexible residue of BtuF over the B_{12}-bound BtuF MD simulation is Gln45 whose RMSF is ca. 0.17 nm. Visualizing all of the four SMD trajectories completely, it is found that two residues, i.e. Gln45 and Trp44, always block the unbinding pathway of B_{12}. Especially the Trp44, which interacts with the B_{12} by its aromatic side chain [11], is the last obstacle for B_{12} to overcome in our SMD simulations. Superimposing the B_{12}-bound structure onto the

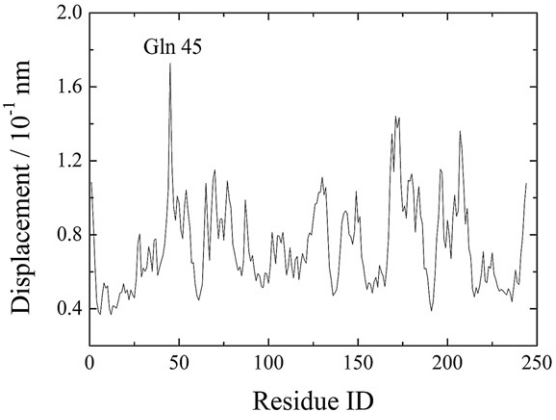

Fig. 6. RMSFs of the C_α atoms of BtuF. Except the expectable large fluctuation in the N and C-terminal, two flexible regions can be found near the B_{12} binding site. The most flexible residue Gln45 is labeled by text.

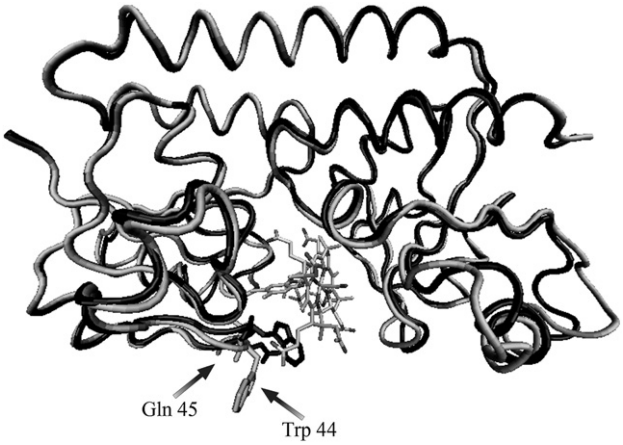

Fig. 7. Superposition of the *holo* and *apo* BtuF. The *holo* BtuF is colored by black and the *apo* BtuF is colored by gray. The (Gln45 and Trp44) are highlighted by the licorice representation in each structure. B12 in the *holo* BtuF is colored by gray and black.

B_{12}-free structure, it's observed that the orientations of the Gln45 and the Trp44 are different between the two states. Both the side chains of the Gln45 and the Trp44 point to the center of the B_{12} binding site (Fig. 7). In particular, the aromatic side chain of Trp44 in the B_{12}-bound state bends to the corrin ring of the B_{12}, whereas this aromatic side chain bends against the corrin ring of the B_{12}. According to these observations, the Trp44 and Gln45seems to act as a gate of the B_{12} binding pocket. After BtuF docking onto the periplasmic side of BtuC, the conformation of the two special residues may change at first to facilitate the unbinding of B_{12}.

The different conformations of the Trp44 in the *apo* and *holo* BtuF remind us the “IN” and “OUT” orientations of the “heme tyrosine” in the two bacterial periplasmic heme binding proteins, i.e. ShuT and PhuT, respectively [41]. The “heme tyrosine”, however, is not an actual gate. The real role of it is to coordinate with the Fe ion at the center of the heme corrin ring thus stabilize the conformation of heme [41]. Again, in the [22], which is closely similar with BtuF in tertiary structure, no gate residues are found either. It seems that the gate residues are not shared by every PBPs of the third class.

Through the sequence alignment of the BtuFs from five different bacteria, it is found that the “gate” is comprised by Trp-Gln in three cases. For the other two sequences, the gate region is substituted by the His-Gln and the Asn-Arg pair, respectively [15]. Though the gate region in BtuF is not highly conserved, the substitutions seem not random. Considering the His-Gln pair, the substitution of His for the former Trp also has an aromatic side chain which may act as that of the Trp. As to the Asn-Arg pair, although the Asn doesn't have an aromatic side chain, the long side chain of it may play a leading role in the postulated “gating mechanism”.

4. Conclusion

In this work, firstly we explored the energetics of B_{12} unbinding from BtuF in virtue of the SMD simulation and the equality of Jarzynski [24]. Suggested by the relatively small fluctuation of the external work, the PMF along the selected pathway is considered as reasonable. Owing to the monotone increasing nature of the PMF, it is likely no favorable interactions that facilitate the unbinding of B_{12} existing along the postulated unbinding pathway. Again, since the free energy change for B_{12} unbinding from BtuF is rather strong, it is suggested the BtuF-B_{12} complex is in a stable closed form, which is consistent with Kandt's results [13]. According to the newly reported crystal structure of the BtuCDF complex [39] and our SMD simulations, BtuF is supposed to undergo a series of conformations changes to facilitate the release of B_{12} after docking onto the periplasmic surface of BtuC.

Secondly, based on the results of PCA, we found even the B_{12}-bound BtuF shows the opening and twisting motion tendency. This property of BtuF may be helpful to the delivery of B_{12}. Finally, the intrinsic flexibility of the BtuF was explored. With the relatively large flexibility, residues such as Trp44, Gln45, Asp169, Arg171, Val172 and Pro173 may play a role in the realistic process of B_{12} unbinding. Especially the Trp44-Gln45 pair, which is located at the mouth of the B_{12} binding pocket, may act as a gate in the B_{12} unbinding process according to the observations on the SMD simulations and the comparison between the *holo* and *apo* crystal structure of BtuF.

Acknowledgement

This work was in part supported by grants from the National Natural Science Foundation of China (No. 30670497 and No. 10574009) and from Beijing Natural Science Foundation (No. 5072002 and No. 7082006).

References

[1] C.B. Felder, R.C. Graul, A.Y. Lee, H.P. Merkle, W. Sadee, The venus flytrap of periplasmic binding proteins: an ancient protein module present in multiple drug receptors, AAPS PharmSci 1 (1999).
[2] R. Tam, M.H.J. Saier, Structural, functional, and evolutionary relationships among extracellular solute-binding receptors of bacteria, Microbiol. Rev. 57 (1996) 320–346.
[3] F.A. Quiocho, P.S. Ledvina, Atomic structure and specificity of bacterial periplasmic receptors for active transport and chemotaxis: variation of common themes, Mol. Microbiol. 20 (1996) 17–25.
[4] W. Köster, ABC transporter-mediated uptake of iron, siderophores, heme and vitamin B12, Res. Microbiol. 152 (2001) 291–301.
[5] A.J.M. Driessen, B.P. Rosen, W.N. Konings, Diversity of transport mechanisms: common structural principles, Trends Biochem. Sci. 25 (2000) 397–401.
[6] J.S. Sack, M.A. Saper, F.A. Quiocho, Periplasmic Binding Protein Structure and Function. Refined X-ray Structures of the Leucine/Isoleucine/Valine-binding Protein and its Complex with Leucine, J. Mol. Biol. 206 (1989) 171–191.
[7] T.E. Clarke, L.W. Tari, H.J. Vogel, Structural biology of bacterial iron uptake systems, Curr. Top. Med. Chem. 1 (2001) 7–30.
[8] M.E. Newcomer, G.L. Gilliland, F.A. Quiochol, J. Biol. Chem. 256 (1981) 13213–13217.
[9] J.C. Spurlino, G.Y. Lu, F.A. Quiocho, The 2.3-Å resolution. Structure of the maltose- or maltodextrin-binding protein, a primary receptor of bacterial active transport and chemotaxis, J. Biol. Chem. 266 (1991) 5202–5219.
[10] K. Fukami-Kobayashi, Y. Tateno, K. Nishikawa, Domain dislocation: a change of core structure in periplasmic binding proteins in their evolutionary history, J. Biol. Chem. 286 (1999) 279–290.
[11] E.L. Borths, K.P. Locher, A.T. Lee, D.C. Rees, The structure of *Escherichia coli* BtuF and binding to its cognate ATP binding cassette transporter, Proc. Natl. Acad. Sci. U. S. A. 99 (2002) 16642–16647.
[12] N. Cadieux, C. Bradbeer, E. Reeger-Schneider, W. Köster, A.K. Mohanty, M.C. Wiener, R.J. Kadner, Identification of the periplasmic cobalamin-binding protein BtuF of *Escherichia coli*, J. Bacteriol. 184 (2002) 706–717.
[13] C. Kandt, Z. Xu, D.P. Tieleman, Opening and closing motions in the periplasmic vitamin B12 binding protein BtuF, Biochemistry 45 (2006) 13284–13292.
[14] D.P. Chimento, A.K. Mohanty, R.J. Kadner, M.C. Wiener, Substrate-induced transmembrane signaling in the cobalamin transporter BtuB, Nat. Struct. Biol. 10 (2003) 394–401.
[15] N.K. Karpowich, H.H. Huang, P.C. Smith, J.F. Hunt, Crystal Structures of the BtuF periplasmic-binding protein for vitamin B12 suggest a functionally important reduction in protein mobility upon ligand binding, J. Biol. Chem. 278 (2002).
[16] K.P. Locher, A.T. Lee, D.C. Rees, The *E. coli* BtuCD structure: a framework for ABC transporter architecture and mechanism, Science 296 (2002) 1091–1098.
[17] D.N. Sheppard, M.J. Welsh, Structure and function of the CFTR chloride channel, Physiol. Rev. 79 (1999) 23–45.
[18] M.M. Gottesman, S.V. Ambudkar, Overview: ABC transporters and human disease, J. Bioenerg. Biomembranes 33 (2001) 453–458.
[19] R. Abele, R. Tampé, Function of the transport complex TAP in cellular immune recognition, Biochim. Biophys. Acta 1461 (1999) 405–419.
[20] H. Nikaido, Prevention of Drug Access to Bacterial Targets: Permeability Barriers and Active Efflux, Science, 264 (1994) 382–388, (Washington, D. C., 1883–).
[21] E.L. Borths, B. Poolman, R.N. Hvorup, K.P. Locher, D.C. Rees, In vitro functional characterization of BtuCD-F, the *Escherichia coli* ABC transporter for vitamin B12 uptake, Biochemistry 44 (2005) 16301–16309.
[22] T.E. Clarke, S.Y. Ku, D.R. Dougan, H.J. Vogel, L.W. Tari, The structure of the ferric siderophore binding protein FhuD complexed with gallichrome, Nat. Struct. Biol. 7 (2000) 287–291.
[23] B.H. Oh, J. Pandit, C.H. Kang, K. Nikaido, S. Gokcen, G.F.-L. Amesll, S.-H. Kim, Three-dimensional structures of the periplasmic lysine/arginine/ornithine-binding protein with and without a ligand, Biochim. Biophys. Acta 268 (1993) 11348–11355.
[24] C. Jarzynski, Equilibrium free-energy differences from nonequilibrium measurements: a master-equation approach, Phys. Rev., E 56 (1997) 5018–5035.
[25] B.R. Brooks, R.E. Bruccoleri, B.D. Olafson, D.J. States, S. Swaminathan, M. Karplus, CHARMM: a program for macromolecular energy, minimization, and dynamics calculations, J. Comput. Chem. 4 (1983) 187–217.
[26] H.M. Marquesa, B. Ngomaa, T.J. Eganb, K.L. Brownc, Parameters for the amber force field for the molecular mechanics modeling of the cobalt corrinoids, J. Mol. Struct. 561 (2001) 71–91.
[27] W. Humphrey, A. Dalke, K. Schulten, VMD: visual molecular dynamics, J. Mol. Graph. 14 (1996) 33–38.
[28] L. Kale, R. Skeel, M. Bhandarkar, R. Brunner, A. Gursoy, N. Krawetz, J. Phillips, A. Shinozaki, K. Varadarajan, K. Schulten, NAMD2: greater scalability for parallel molecular dynamics, J. Comput. Phys. 151 (1999) 283–312.
[29] A.D.J. MacKerell, D. Bashford, M. Bellott, J.R.L. Dunbrack, All-atom empirical potential for molecular modeling and dynamics studies of proteins, J. Phys. Chem., B 102 (1998) 3586–3616.
[30] S.E. Feller, Y. Zhang, R.W. Pastor, B.R. Brooks, constant pressure molecular dynamics simulation: the Langevin Piston Method, J. Chem. Phys. 103 (1995) 4613–4621.
[31] S. Park, F. Khalili-Araghi, E. Tajkhorshid, K. Schultena, Free energy calculation from steered molecular dynamics simulations using Jarzynski's Equality, J. Chem. Phys. 119 (2003) 3559–3566.
[32] S. Park, K. Schulten, Calculating potentials of mean force from steered molecular dynamics simulations, J. Chem. Phys. 120 (2004) 5946–5961.
[33] A. Amadei, A.B.M. Linssen, D.H.J.C. Berendsen, Essential dynamics of proteins, proteins, Struct. Funct. Genet. 17 (1993) 412–425.
[34] H.J.C. Berendsen, D. vanderSpoel, R. vanDrunen, Gromacs: a message-passing parallel molecular-dynamics implementation, Comput. Phys. Commun. 91 (1995) 43–56.
[35] C. Jarzynski, Nonequilibrium equality for free energy differences, Phys. Rev. Lett. 78 (1997) 2690–2693.
[36] J. Liphardt, S. Dumont, S.B. Smith, I.T. Jr, C. Bustamante, Equilibrium Information from nonequilibrium measurements in an experimental test of Jarzynski's Equality, Science 296 (2002) 1832–1835.
[37] G. Hummer, A. Szabo, Free energy reconstruction from nonequilibrium single-molecule pulling experiments, Proc. Natl. Acad. Sci. U. S. A. 98 (2001) 3658–3661.
[38] J. Sonne, C. Kandt, G.N.H. Peters, F.Y. Hansen, Z. Morten, Ø. Jensen, D.P. Tieleman, Simulation of the coupling between nucleotide binding and transmembrane domains in the ATP Binding cassette transporter BtuCD, Biophys. J. 92 (2007) 2727–2734.
[39] R.N. Hvorup, B.A. Goetz, M. Niederer, K. Hollenstein, E. Perozo, K.P. Locher, Asymmetry in the structure of the ABC transporter-binding protein complex BtuCD-BtuF, Science 317 (2007) 1387–1390.
[40] A. Ivetac, J.D. Campbell, M.S.P. Sansom, Dynamics and function in a bacterial ABC transporter: simulation studies of the BtuCDF system and its components, Biochemistry 46 (2007) 2767–2778.
[41] W.W. Ho, H. Li, S. Eakanunkul, Y. Tong, A. Wilks, M. Guo, T.L. Poulos, Holo- and Apo-structures of bacterial periplasmic heme binding proteins, J. Biol. Chem. 282 (2007) 35796–35802.